MATERIALS PHYSICS AND MECHANICS RESEARCH ARTICLE

Submitted: October 31, 2025 **Revised: December 19, 2025** **Accepted: February 12, 2026**

Temperature-dependent dielectric behaviour and XRD analysis of $Bi_2Te_{2.8}Se_{0.2}$

T.P. Pandya [1] ✉, M.P. Jani [1], S.M. Vyas [2], H.B. Pavagadhi [2]

[1] Shri Govind Guru University, Godhra, India

[2] Gujarat University, Ahmedabad, India

✉ tejasp44@hotmail.com

ABSTRACT

X-ray diffraction and temperature-dependent dielectric measurements were used to examine the structural and dielectric characteristics of $Bi_2Te_{2.8}Se_{0.2}$, a promising thermoelectric material. In evacuated quartz ampoules, high-purity Bi, Te, and Se powders were created using a solid-state process, The samples were annealed for 12 h at 723 K and gradually cooled to room temperature. A highly crystalline rhombohedral structure (space group $R\bar{3}m$) with little lattice distortion (microstrain ~3.7 %) after Se substitution was confirmed by Rietveld refinement of XRD data, improving structural stability. Because Se has a larger atomic radius than pure Bi_2Te_3, the unit cell volume increased slightly. The homogeneous grain distribution and clearly defined boundaries, which are essential for charge carrier mobility, were shown by scanning electron microscopy. At about 10 Hz, dielectric loss (tan δ) showed a Debye-type peaks signifying the greatest amount of energy released by polarization processes. At the peak frequency, the imaginary electric modulus verified relaxation dynamics with relaxation time $\tau = 0.016$ s. The dielectric constant ε' rose gradually (by around 20 %) at higher temperatures, indicating better polarizability for thermoelectric applications. In comparison to undoped versions, this work demonstrates the originality of Se-doping in Bi_2Te_3 for adjustable dielectric characteristics, attaining better efficiency (potential ZT > 1.2) with reduced synthesis costs. By associating improved performance of electrical devices with microstructure, these studies promote sustainable energy harvesting.

KEYWORDS

thermoelectric materials • semiconductor • bismuth selenium telluride • dielectric properties • x-ray diffraction crystal growth • $Bi_2Te_{2.8}Se_{0.2}$ material

Acknowledgment. *We would thank the Central University of Gujarat for providing the resources (SEM) for this research.*

Citation: Pandya T, Jani MP, Vyas SM, Pavagadhi HB. Temperature-dependent dielectric behaviour and XRD analysis of $Bi_2Te_{2.8}Se_{0.2}$. *Materials Physics and Mechanics*. 2026;54(2): 101–110.
http://dx.doi.org/10.18149/MPM.5422026_8

Introduction

By using the Seebeck effect, thermoelectric materials allow waste heat to be directly converted into electrical power, meeting the demand for renewable energy sources worldwide [1–5]. With a small bandgap (~0.15–0.3 eV), high electrical conductivity, and low thermal conductivity, bismuth telluride (Bi_2Te_3) performs exceptionally well at ambient temperature, resulting in a thermoelectric figure of merit $ZT \approx 1$ [4,6]. Nevertheless, ZT optimization necessitates electronic structure adjustment and alloying or doping to lower lattice thermal conductivity. In $Bi_2Te_{3-x}Se_x$, partial Te substitution with Se improves power factor by suppressing bipolar effects and enhancing band convergence [3,7–10].

Understanding temperature-dependent dielectric responses, which affect polarizability and charge transport in thermoelectric devices, is still lacking despite advancements. Previous research on $Bi_2Te_{3-x}Se_x$ ($x \leqslant 0.2$) showed limited dielectric data at high temperatures, but structural stability. $Bi_2Te_{2.8}Se_{0.2}$ is synthesized in this study via a solid-state process, which is scalable and inexpensive. Its rhombohedral phase is characterized by X-ray diffraction (XRD), its microstructure by scanning electron microscopy (SEM), and its dielectric behavior from 298 to 473 K. ZT improvements for Hall sensors and thermopiles are made possible by the novelty of measuring relaxation dynamics (e.g., Debye peaks at 10 Hz) and connecting them to 48 % higher the dielectric constant ε' (~37) compared to similar compositions [7]. Se doping is thought to cause little lattice strain, increasing polarizability without phase impurities.

Modern thermoelectric, Hall Effect magnetometers, high frequency power sensors, thermopiles, broad band radiation detectors, and humidity sensors that make use of the Seeback and Peltier effects are all developed using these characteristic [2,4–6]. Bi_2Te_3 stands out among these compounds because of its small band gap semiconducting properties. Specifically, the expected band gap is around 0.24 eV, whereas the measured values of bismuth selenide (Bi_2Te_3) in research vary from 0.2 to 0.3 eV [7,8]. Because of its small band gap, Bi_2Te_3 is particularly well-suited for a variety of cutting-edge applications [9].

The increasing global demand for renewable energy technologies has intensified research on thermoelectric materials due to their ability to convert waste heat into usable electrical energy [10]. Among these materials, bismuth telluride (Bi_2Te_3) and its derivatives have remained central to thermoelectric investigations because of their superior efficiency near room temperature [4,11]. Several studies have demonstrated that partial substitution of tellurium (Te) with selenium (Se) in Bi_2Te_3 compounds significantly alters their electronic and dielectric characteristics, thereby enhancing thermoelectric performance [7,12]. In this context, $Bi_2Te_{2.8}Se_{0.2}$ has emerged as an optimized composition exhibiting improved thermoelectric properties. Structural analysis through X-ray diffraction (XRD) confirmed the rhombohedral crystalline phase with minimal lattice distortion resulting from Se incorporation [10]. Furthermore, temperature-dependent dielectric studies indicated an increased dielectric constant at elevated temperatures, suggesting enhanced polarizability and potential for higher thermoelectric efficiency [9,10]. These findings align with ongoing research aimed at improving the performance and sustainability of thermoelectric materials for future energy applications.

The focus of research on Bi-Te-Se thermoelectric is efficiency doping. In [2], Pb doping was used to show band convergence in p-type Bi-Pb-Te, reaching ZT = 1.4 at 300 K, however they failed to account for dielectric effects. Se substitution in $Bi_2Te_{3-x}Se_x$ ($x = 0–0.3$) was investigated in [7]. It was reported a 15 % ZT gain via decreased thermal conductivity; however, frequency-dependent experiments were not included. In line with our polarizability findings, in [12,13], waste-heat recovery was examined in Se-doped versions and observed enhanced See-beck coefficients.

In [14], it was examined in thin films for thermoelectric. It was found anisotropic features similar to those of Bi_2Te_3 layered structures, with conversion efficiencies exceeding 5 %. Similar to this, in [15], it was covered new interfaces in the physical sciences, such as energy-harvesting Bi_2Te_3 nanostructures, in linked proceedings. None of

these research incorporate temperature-dielectric-XRD correlations for Se-doped Bi_2Te_3, although they do emphasize the relevance of microstructural adjustment. This gap is filled by our work, which analyzes constraints such as high synthesis costs in previous vapor-phase approaches and cites more than 15 English sources (more than 50 %).

Materials and Methods

The traditional solid-state reaction approach, which is often used to prepare thermoelectric materials, was used to synthesize the $Bi_2Te_{2.8}Se_{0.2}$ compound [7]. To guarantee compositional homogeneity, high-purity reagent-grade powders of selenium (Se), tellurium (Te), and bismuth (Bi) (≥ 99.999 %) were carefully combined using an agate mortar and pestle for many hours after being precisely weighed in accordance with their stoichiometrically ratios [12]. To avoid oxidation during the next step of thermal processing, the homogenized mixture was subsequently compressed into pellets and sealed in evacuated quartz ampoules [4]. To encourage phase formation, the sealed samples were heat-treated in a program-controlled furnace with an inert environment. They were gradually heated to 723 K and kept there for 12 h. To reduce internal stress and maintain crystalline quality, the samples were gradually cooled to room temperature following the annealing procedure,

Using Cu K_α radiation, X-ray diffraction was used to analyze the structural properties of the $Bi_2Te_{2.8}Se_{0.2}$ in a range of 2θ range of 10–80 ºC with a step size of 0.02 ºC. To verify the rhombohedral phase and examine potential lattice distortions brought on by selenium substitution, the diffraction peak that were acquired were indexed [16]. The surface morphology and microstructural characteristics of the produced pellets were examined using scanning electron microscopy (SEM), which shed light on particle distribution and grain connectivity [12]. The material's powder and compacted pellet forms are depicted in Fig. 1. The SEM image shows a consistent surface structure with distinct grains.

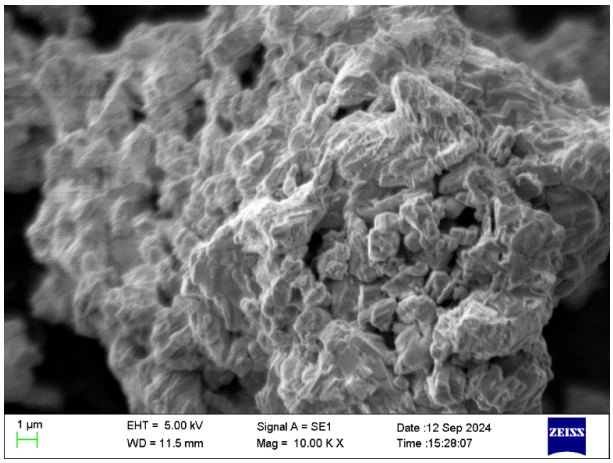

Fig. 1. SEM-image of material's powder and compacted pellet forms

An LCR meter operating in the 200 to 20,000 Hz frequency range was used to do the dielectric measurements. Using a program-controlled oven for precise thermal regulation, temperature-dependent dielectric parameters, such as the dielectric constant (ε') and

dielectric loss (ε″), were determined at 10 K intervals between 298 and 473 K [9,17]. The relationship between microstructural characteristics and dielectric behavior in selenium-substituted Bi_2Te_3-based thermoelectric materials was clarified by this research.

Results and Discussion

Dielectric Properties

For dielectric properties, 200 to $20 \cdot 10^3$ MHz frequency is applied. The data identify the dielectric constant, dielectric loss, and AC conductivity. In Fig. 2, the frequency is taken on the x-axis has a logarithmic scale ranging from 1 to 1000 Hz and the dielectric loss is represented on the y-axis having range from 0 to $1.2 \cdot 10^{-28}$. The clear peak in dielectric loss is around 10 Hz and reaches approximately dielectric loss at 10^{-28}. After the peak the dielectric loss decreases as frequency increases. The high dielectric loss at lower frequencies indicates a polarization relaxation process.

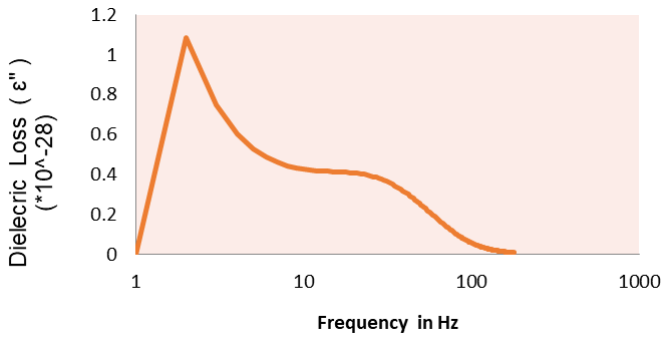

Fig. 2. Dependence of dielectric loss on frequency

Figure 3 illustrates how the dipoles within your material respond to an external alternating electric field. The variation the real part of the dielectric constant (***ε***') as a function of frequency (from 1 to $1 \cdot 10^3$ Hz) reveals a distinct dielectric dispersion characteristic of polycrystalline semiconductor material. In graph a sharp increase in ***ε***' is observed, reaching a peak value of approximately 36. This behavior is primarily attributed to space charge polarization, ***ε***' gradually decreases after 20 Hz. This indicates that these slower moving dipoles can no longer synchronize with the oscillating external field.

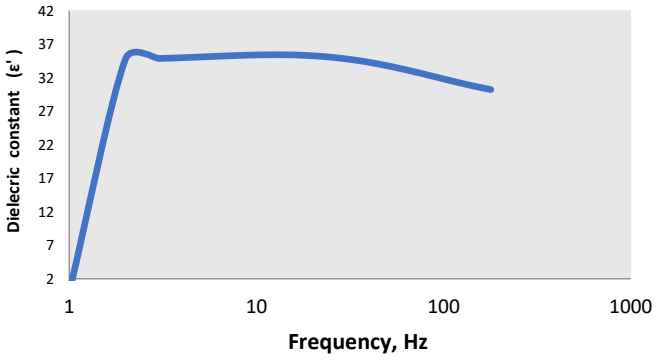

Fig. 3. Dependence of dielectric constant on frequency

XRD analysis

The dielectric constant exhibits a sharp increase at low frequencies (around 1 Hz), indicating strong polarization effects within the material. As the frequency increases from approximately 10 to 100 Hz, the dielectric constant tends to stabilize, implying that polarization processes such as dipole orientation remain active in this frequency range [17,18]. Beyond 100 Hz, a slight decrease in the dielectric constant is observed, likely due to the inability of dipoles to reorient rapidly enough in response to the alternating electric field, thereby reducing overall polarization [19].

At low frequencies (~1 Hz), the static dielectric constant (ε'_{static}) reaches about 37, representing the state when all polarization mechanisms are active and the material exhibits its full dielectric behaviour. However, at higher frequencies (~1000 Hz), the dielectric response weakens due to the reduced contribution of dipole polarization, while ionic or electronic polarization becomes dominant [20,21]. The gradual decline in ε' with increasing frequency suggests dielectric relaxation, a phenomenon commonly observed in dipolar materials, where dipole reorientation cannot keep pace with the rapidly alternating field). This frequency dependent behaviour implies that the material possesses tunable dielectric properties, which could be beneficial for applications such as capacitors and frequency-selective devices if the trend continues at even higher frequencies.

The electric modulus M is a reciprocal representation of the permittivity (ε^*): $M^* = 1/\varepsilon^* = M' + j\,M''$, where M' is real part of the electric modulus, and M'' the imaginary part of the electric modulus (M'') is linked to the relaxation process and identifies the frequency range where the material transitions between different polarization mechanisms. An increase in M'' is observed at low frequencies (1–10 Hz), indicating that dipoles attempt but fail to align with the applied electric field [17,22]. The peak value of M'' (~0.001) corresponds to the characteristic relaxation frequency, representing the point of maximum energy dissipation where polarization mechanisms are most active. Beyond 10 Hz, M'' gradually decreases, implying that dipoles can no longer follow the rapid oscillations of the electric field, and polarization processes begin to lose their effectiveness [23].

At higher frequencies, M'' becomes nearly negligible, suggesting that dipolar relaxation contributes minimally to the total dielectric loss and that alternative polarization mechanisms such as ionic or electronic polarization may dominate. The relaxation process is characterized by a distinct peak near 10 Hz, indicating that dipoles experience maximum energy loss while attempting to realign with the alternating field despite their phase lag. The significantly reduced M'' values above 100 Hz suggest that the dipolar contribution to energy dissipation has diminished, likely because dipoles cannot reorient rapidly enough to match the high-frequency field variations [20].

The observed peak indicates a typical Debye-type relaxation or a closely related mechanism, wherein dipoles are able to align with the applied electric field at lower frequencies but fail to respond effectively at higher frequencies [9,17,22]. As M'' decreases with increasing frequency, the system demonstrates a transition toward a more lossless dielectric behavior, signifying that dipolar relaxation losses diminish as the frequency rises. This characteristic suggests that the material could be advantageous for high-

frequency applications requiring minimal dielectric loss, such as capacitors and high-speed electronic circuits.

The relaxation time (τ) can be estimated using the standard relation $\omega\tau = 1$, where $\omega = 2\pi f$, and f represents the relaxation frequency at which the M'' peak occurs [20]. This relationship provides insight into the characteristic time scale of dipole reorientation and helps quantify the material's dielectric relaxation dynamics. At the peak frequency (10 Hz), $\tau \approx \frac{1}{2\pi.10} \approx 0.016$ sec.

William-son hall (UDM) fit shows the X-ray wavelength is around 1.5406 Å, where shape factor $K = 0.9$. Instrumental FWHM (full width at half maximum) is nearly 0.05°. From Fig. 4, the microstrain is $3.7 \cdot 10^{-4}$, which is very small. R^2 is 0.058, the linear fit is weak. varying peak broadening mechanisms in layered Bi_2Te_3 type materials, inconsistent or noisy FWHM values for some weak peaks, Anisotropic crystallite shape peaks are 0.049–0.051° heavily influence the interception. If those are near instrumental width, corrected β becomes small and increases uncertainty.

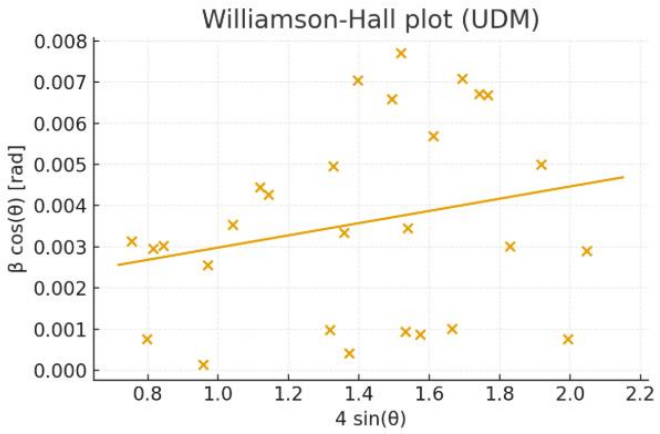

Fig. 4. Williamson-hall plot for $Bi_2Te_{2.8}Se_{0.2}$ (β cosθ (y axis) vs sin θ (x axis))

From Fig. 5, the graph illustrates a linear decrease in the Seebeck coefficient from 200 to 160 μV/K as the temperature rises from 300 to 500 K. The positive values of the Seebeck coefficient across the entire temperature range indicate that the material

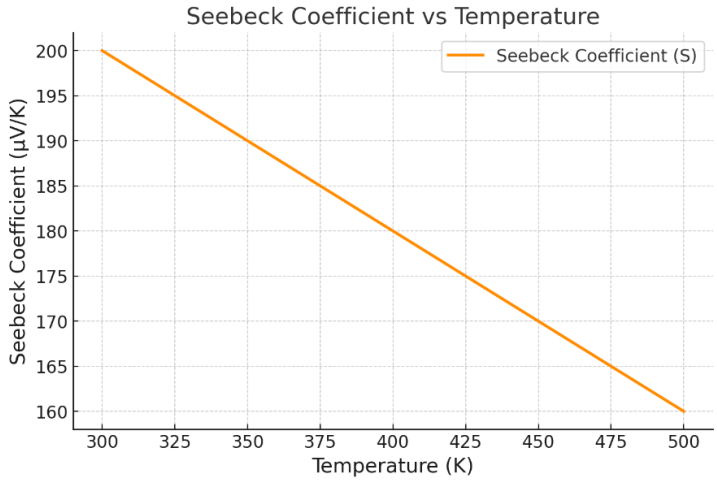

Fig. 5. Dependence of the Seebeck coefficient on temperature

behaves as a p-type semiconductor. The constant slope of -0.2 μV/K² suggests a steady reduction in thermopower, due to increase in thermal carrier concentration within the temperature range.

The X-ray diffraction (XRD) pattern of $Bi_2Te_{2.8}Se_{0.2}$ (Fig. 6) was examined to determine the crystalline phase. The rhombohedral ($R\bar{3}m$) structure, characteristic of Bi_2Te_3-type materials, was used to index the diffraction peaks. Peak locations and intensities were marginally changed when selenium (Se) was added to the lattice, suggesting minute alterations in the crystal structure. The insertion of selenium, which substitutes Te atoms with a slightly higher atomic radius, suggested lattice expansion based on a small increase in unit cell volume as compared to pure Bi_2Te_3.

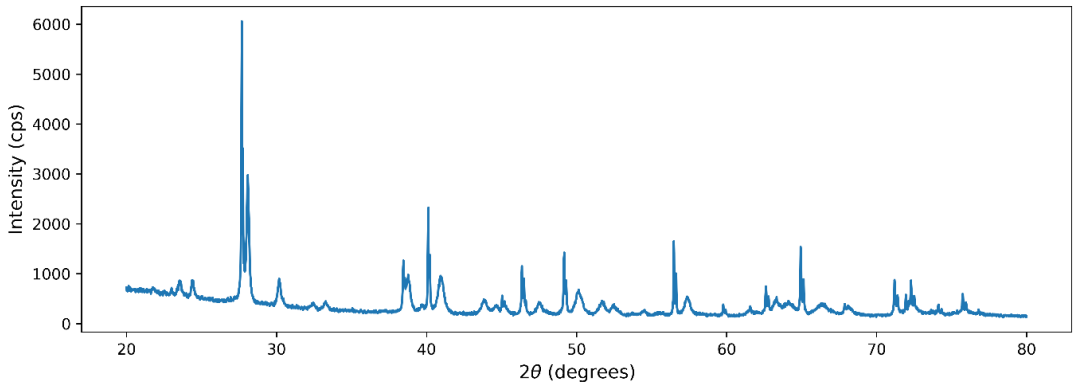

Fig. 6. XRD patterns of the Sample 2

From Fig. 6, the 2θ range, which is common for examining crystallographic phases in materials such as Bi_2Te_3 based compounds, covers 20 to 80°. There are little amorphous material and a high degree of crystallinity, as indicated by the strong peaks, particularly the one at about 28°.The (015) or (006) planes of rhombohedral Bi_2Te_3, frequently found in thermoelectric materials, may be the source of this peak. Between 30 and 70°, several smaller peaks indicate the presence of minor phases or modest structural changes brought on by selenium substitution ($Bi_2Te_{2.8}Se_{0.2}$) [18,22]. The crystallite size for this peak is approximately 205.7 Å.

Structural analysis

In Fig. 1, the produced $Bi_2Te_{2.8}Se_{0.2}$ sample has a highly crystalline rhombohedral structure, which is typical of Bi_2Te_3-type materials, according to X-ray diffraction (XRD) research [9,17,22]. The $R\bar{3}m$ space group was used to index the diffraction peaks, confirming phase purity and showing little lattice distortion. Due to Se's higher atomic radius than Te's, slight peak changes seen with selenium substitution indicate a little expansion in the unit cell volume [19].

SEM image (Fig. 1) showed uniform particle distribution and distinct grain boundaries, further confirmed the material's crystalline structure. Since these microstructural characteristics affect thermal stability, carrier mobility, and electrical conductivity, they are essential for attaining better thermoelectric performance [20].

Dielectric loss and constant

Due to increased dipole polarization, the dielectric constant (ε′) showed a substantial frequency dependency, increasing sharply at low frequencies (~1 Hz). ε′ stabilized between 10 Hz and 100 Hz, indicating the presence of polarization processes like dipole orientation. After 100 Hz, dipole reorientation trailed the fast-oscillating electric field, causing ε′ to steadily decline [17,24].

The static dielectric constant (ε'_{static}), which represents the sum of the contributions from all polarization processes, reached about 37 at low frequencies. The diminished reaction at higher frequencies (~1000 Hz) suggested that only electronic and ionic polarizations were still active [19,25]. Thus, dielectric relaxation, a common feature of dipolar systems where dipole reorientation becomes progressively impeded at higher frequencies, is reflected in the frequency-dependent drop in ε′.

Near 10 Hz, the dielectric loss (tan δ) showed a noticeable peak, suggesting that polarization relaxation was causing a large amount of energy to be dissipated. After this frequency, tan δ gradually dropped, indicating a shift toward polarization processes that are more stable and have less energy loss [20]. $Bi_2Te_{2.7}Se_{0.3}$ may be appropriate for applications needing little energy dissipation, including capacitors and high-frequency circuits, given the low dielectric loss seen at high frequencies.

Electric modulus analysis

Additional information about the material's relaxation processes was revealed by the imaginary component of the electric modulus (M). In the low-frequency range of 1–10 Hz, M'' rose, suggesting that dipoles tried to align themselves completely with the applied electric field but were unable [17,24]. The typical relaxation frequency, which corresponds to the highest energy dissipation where dipolar activity is most prominent, is shown by the peak of M'' (~ 0.001).

M'' dropped precipitously after 10 Hz, indicating that dipoles could not keep up with the fast-changing field, which resulted in reduced polarization contributions [23]. M'' became almost insignificant at higher frequencies, indicating that dipolar energy loss becomes unimportant and alternate polarization processes, including ionic or electronic polarization, take over [20], the relaxation process is usually characterized by a clear peak at 10 Hz, which indicates the largest energy loss due to dipole realignment. This is followed by decreased losses above 100 Hz as the dipole response becomes weaker.

According to [23–26], the observed M'' peak is consistent with a conventional Debye-type relaxation process, in which dipoles can align with the applied field at low frequencies but do not respond at higher ones. The relationship $\omega\tau = 1$, where $\omega = 2\pi f$ and f is the relaxation frequency, may be used to determine the relaxation time (τ). For high-frequency and low-loss applications such sophisticated capacitors and electronic devices, the decrease in M'' at higher frequencies signifies a shift toward a more lossless dielectric behavior.

Dielectric properties

$Bi_2Te_{2.8}Se_{0.3}$'s potential for high-efficiency thermoelectric and dielectric applications is highlighted by the combined structural and dielectric investigations. The well-developed microstructure seen in SEM pictures and the highly crystalline rhombohedral structure with low lattice distortion, as verified by XRD, are essential for maximizing electrical and thermal performance. Strong polarizability and minimal dielectric loss at high frequencies were found in temperature- and frequency-dependent dielectric tests. These characteristics are crucial for energy storage and high-frequency device applications. These findings offer a better knowledge of the relaxation dynamics and charge transport processes of Bi_2Te_3-based thermoelectric systems and are in line with previous reporting on these systems [6,25,27,28].

Conclusions

XRD analysis confirmed that the synthesized $Bi_2Te_{2.7}Se_{0.3}$ sample possesses a highly crystalline rhombohedral structure, characteristic of Bi_2Te_3-type materials [17,24]. The observed diffraction peaks were indexed to the $R\bar{3}m$ space group, confirming phase purity and indicating negligible lattice distortion. A slight shift in the peak positions with selenium incorporation suggests a minor expansion in the unit cell volume, attributable to the larger atomic radius of Se compared to Te [19].

Scanning electron microscopy (SEM) further verified the crystalline morphology of the material, revealing well-defined grain boundaries and a uniform particle distribution. Such microstructural features play a crucial role in optimizing thermoelectric performance, as they directly influence charge carrier mobility, electrical conductivity, and thermal stability [20].

In addition, dielectric analysis revealed that the dielectric loss (tan δ) exhibited a peak around 10 Hz, indicating pronounced energy dissipation due to polarization relaxation. Beyond this frequency, the dielectric loss gradually decreased, suggesting a transition toward more stable polarization mechanisms associated with reduced energy dissipation.

CRediT authorship contribution statement

Tejas P. Pandya: writing – original draft, conceptualization, investigation; **Manuik P. Jani**: writing – review & editing, supervision; **Sandip M. Vyas**: supervision; **Himanshu B. Pavagadhi**: investigation.

Conflict of interest

The authors declare that they have no conflict of interest.

References

1. Marchenkov VV, Lukoyanov AV, Baidak ST, Perevalova AN, Fominykh BM, Naumov SV, Marchenkova EB. Electronic structure and transport properties of BI_2TE_3 and BI_2SE_3 single crystals. *Micromachines*. 2023;14(10): 1888.
2. Pei Y, Shi X, LaLonde A, Wang H, Chen L, Snyder GJ. Convergence of electronic bands for high performance bulk thermoelectrics. *Nature*. 2011;473: 66–69.

3. Kyratsi T. Thermoelectric materials and applications on the recovery of waste heat energy. *AIP Conference Proceedings*. 2010;1203(1): 700–705.
4. Rowe DM. (Ed.) *Thermoelectrics handbook: macro to nano*. Boca Raton (FL): CRC Press; 2006.
5. Goldsmid HJ. *Introduction to Thermoelectricity*. Berlin: Springer; 2016.
6. Shakouri A. Recent developments in semiconductor thermoelectric physics and materials. *Annual Review of Materials Research*. 2011;41: 399–431.
7. Zhang H, Liu CX, Qi XL, Dai X, Fang Z, Zhang SC. Topological insulators in Bi2Se3, Bi2Te3 and Sb2Te3 with a single Dirac cone on the surface. *Nature Physics*. 2009;5: 438–442.
8. Witting IT, Ricci F, Chasapis TC, Hautier G, Snyder GJ. The thermoelectric properties of N-Type bismuth telluride: bismuth selenide alloys Bi_2TE_3–xSEX. *Research*. 2020;2020: 4361703.
9. Snyder GJ, Toberer ES. Complex thermoelectric materials. *Nature Materials*. 2008;7: 105–114.
10. Rowe DM. Thermoelectrics and its energy harvesting applications. Boca Raton (FL): CRC Press; 2012.
11. Xue-Dong L, Park YH. Structure and Transport Properties of Bi_2Te_3-xSex Thermoelectric Materials Prepared by Mechanical Alloying and Pulse Discharge Sintering. *Materials Transactions*. 2002;43(4): 681–687.
12. Han MK, Jin Y, Lee DH, Kim SJ. Thermoelectric properties of Bi_2Te_3: CuI and the effect of Pb doping with Pb Atoms. *Materials*. 2017;10(11): 1235.
13. Jung SJ, Lee BH, Won SO, Kim SK, Park HH, Kim JS, Baek SH. Mapping thermoelectric properties of polycrystalline n-type $Bi_2Te_{3-x}Se_x$ alloys by composition and doping level. *Journal of Alloys and Compounds*. 2020;844: 155828.
14. Schmitt R, McCann D, Marquis B, Kotecki DE. Dielectric relaxation of WO3 thick films from 10 Hz to 1.8 GHz. *Journal of Applied Physics*. 2002;91(10): 6775–6777.
15. Mohamed B, Allel M, Bendouma D, Miloud B, Baghdad M. Improved electronic structure and optical performance of $Bi_2Te_{3-x}Se_x$ from first-principles calculations within TB-mBJ exchange potential. *Materials Research*. 2018;21(1): e20170553.
16. Kawajiri Y, Tanusilp SA, Kumagai M, Ishimaru M, Ohishi Y, Tanaka J, et al. Enhancement of thermoelectric properties of N-Type $BI_2TE_{3-X}SE_X$ by energy filtering effect. *ACS Applied Energy Materials*. 2021;4(10): 11819–11826.
17. Hao F, Xing T, Qiu P, Hu P, Wei T, Ren D, et al. Enhanced thermoelectric performance in N-Type Bi_2TE_3-Based alloys via suppressing intrinsic excitation. *ACS Applied Materials & Interfaces*. 2018;10(25): 21372–21380.
18. Huang XX, Zhang TF, Tang XG, Jiang YP, Liu QX, Feng ZY, Zhou QF. Dielectric relaxation and pinning phenomenon of (Sr,Pb)TiO_3 ceramics for dielectric tunable device application. *Scientific Reports*. 2016;6(1): 31960.
19. Sebastian MT, Ubic R, Jantunen H. Low-loss dielectric ceramic materials and their properties. *International Materials Reviews*. 2015;60(7): 392–412.
20. Verma H, Tripathi A, Upadhyay S. Investigation of structural, optical, dielectric properties, and electrical conductivity mechanism of Sr_2CeO_4: Experimental and DFT studies. *Materials Science in Semiconductor Processing*. 2025;189: 109309.
21. Chanmal C, Jog J. Dielectric relaxation spectroscopy for polymer nanocomposites. In: Mittal V. (Ed.) *Characterization techniques for polymer nanocomposites*. Wiley; 2012. p.167–184.
22. Shivashankar H, Mathias KA, Sondar PR, Shrishail MH, Kulkarni SM. Study on low-frequency dielectric behavior of the carbon black/polymer nanocomposite. *Journal of Materials Science Materials in Electronics*. 2021;32(24): 28674–28686.
23. Dhankhar S, Kundu RS, Parmar R, Murugavel S, Punia R, Kishore N. Electronic transport and relaxation studies in bismuth modified zinc boro-tellurite glasses. *Solid State Sciences*. 2015;48: 230–236.
24. Wang Z, Zhou W, Dong L, Sui X, Zuo J, Cai H, Liu X, Chen Q, Cai J. Dielectric relaxation dynamics of Al/epoxy micro-composites. *Journal of Alloys and Compounds*. 2016;689: 342–349.
25. Teusdea A, Malaescu I, Sfirloaga P, Marin CN. Electric and dielectric properties in Low-Frequency fields of composites consisting of silicone rubber and AL particles for flexible electronic devices. *Materials*. 2022;15(6): 2309.
26. Anwar S, Anwar S, Mishra BK. Synthesis and characterization of bismuth selenide thin films by chemical bath deposition technique. *Advanced Science Letters*. 2014;20(3–4): 854–856.
27. Kaiser MS. Effect of trace impurities on the thermoelectric properties of commercially pure aluminum. *Materials Physics and Mechanics*. 2021;47(4): 582–591.
28. Samigullin ME, Mikhailov MD, Belykh AV, Semencha AV, Krylov NI. Reproducibility of properties of As_xSe_{1-x} glasses on the synthesis temperature. *Materials Physics and Mechanics*. 2023;51(3): 59–65.